

Far-infrared excitations in a quantum antidot at finite magnetic fields

Agustí Emperador, Martí Pi, and Manuel Barranco

*Departament d'Estructura i Constituents de la Matèria, Facultat de Física,
Universitat de Barcelona, E-08028 Barcelona, Spain*

Enrico Lipparini

Dipartimento di Fisica, Università di Trento, and INFM, sezione di Trento. 38050 Povo, Italy

Llorenç Serra

*Departament de Física, Facultat de Ciències,
Universitat de les Illes Balears, E-07071 Palma de Mallorca, Spain
(November 20, 2018)*

Abstract

We have investigated the far-infrared dipole modes of a quantum antidot submitted to a perpendicularly applied magnetic field B . The ground state of the antidot is described within local spin-density functional theory, and the spectrum within time-dependent local spin-density functional theory. The results are compared with those corresponding to a quantum dot of similar electronic surface density. The method is able to reproduce two of the more salient experimental features, namely that main bulk and edge modes have the same circular polarization, and that the negative B dispersion edge branch oscillates, having minima at the B values corresponding to fully occupied Landau levels. It fails, however, to yield the unique feature of short-period antidot lattices that the energy of the edge magnetoplasmon approaches the cyclotron frequency for small B . The existence of anticyclotron polarized bulk modes is discussed, and a detailed account of the dipole spin mode is presented.

PACS 73.20.Dx, 73.20.Mf, 78.20.Bh

I. INTRODUCTION

The far-infrared (FIR) spectroscopy of laterally confined superlattices in the two dimensional electron gas (2DEG) made of holes surrounded by electrons, called antidots, has uncovered^{1–3} a very peculiar behavior of the collective spectrum of these systems. It has been found^{1,2} that it consists of a high frequency branch which starts either with a negative magnetic field (B) dispersion in the case of high electronic surface density n_s , or with a rather flat B dispersion at low n_s , that eventually converges to the cyclotron energy at high B 's, plus a low frequency branch which at high B 's corresponds to the usual edge magnetoplasmon, but that approaches the cyclotron frequency for small magnetic fields. Anticrossing of the modes appears as B increases. It is worth to recall that the mentioned behavior of the high frequency branch is also a feature of the FIR spectrum of quantum rings^{4,5}.

A study employing circularly polarized radiation⁶ has shown that both edge and bulk magnetoplasmons in antidots exhibit the same circular polarization, in contradistinction with what is found in quantum dots^{7,8}. Interestingly, a very recent experiment⁹ has detected weak bulk modes anticyclotron-like polarized, whose existence had been predicted some time ago^{10,11}.

Another difference with dots appeared after a careful analysis of the edge magnetoplasmon¹²: the frequency of this mode shows a conspicuous oscillation with B that has maxima at fully occupied Landau levels (even filling factors ν) in the case of dots, and at half-filled Landau levels (odd ν 's) in the case of antidots.

Several theoretical descriptions of FIR modes in antidots have been given in the past. Some are based on hydrodynamical^{10,13} or classical electrodynamics^{11,14} models, which either do not take into account the periodicity of the antidot array¹³, or which take it into account either in a circularly symmetric Wigner-Seitz approximation¹⁰, or incorporate the parameters of the experimental short-period antidot lattices without further approximations¹⁴.

Despite that all these models have somehow successfully reproduced the FIR absorption in antidots, the interest in achieving a more microscopic description of the ground state (gs) and FIR response still remains. Quantum mechanical (Hartree) models have been set up which take into account the periodicity of the lattice using confining potentials of different complexity^{15–17}. The difficulties inherent to the handling of many single particle (sp) wave functions and realistic confining potentials which reflect the actual antidot lattice have hampered these microscopic methods to achieve a quantitative description of the FIR absorption in antidots, although some features of the process are qualitatively described^{15,17}.

Recently, we have applied a local spin-density functional (LSDFT) method to calculate the structure of isolate antidots at $B = 0$, together with a sum rule approach to describe their FIR spectrum¹⁸. Our aim here is to extend these calculations to the case of finite magnetic fields and to present an account of the gs and dipole response of an antidot within the frame of LSDFT and its time-dependent generalization (TDLSDFT). We recall that these formalisms incorporate the spin degree of freedom and allow to selfconsistently include exchange and correlation effects in the study of the gs and the response of the system, whose importance in the description of 2D electronic structures is nowadays well established.

Rather than isolated antidots, the systems described in this work should be considered as representing long-period antidot lattices. Although no much differences are expected to

appear between the ground state structure of an isolated antidot and that of an antidot in a long-period array, apart from the obvious changes at the border of the unit cell, bulk magnetoplasmons are qualitatively different in both cases¹¹.

II. THE LSDFT AND TDLSDFT APPROACHES

We have modeled an antidot of radius R in a 2DEG of surface density n_s by a positive jellium background of density $n_J(r) = n_s \Theta(r - R)$. The gs of the antidot is obtained solving the Kohn-Sham (KS) equations. The problem is simplified by the imposed circular symmetry, which allows one to write the single particle (sp) wave functions as $\phi_{nl\sigma}(r, \theta) = u_{nl\sigma}(r)e^{-il\theta}$ with $l = 0, \pm 1, \pm 2, \dots$, being $-l$ the sp orbital angular momentum.

We have used effective atomic units defined by $\hbar = e^2/\epsilon = m = 1$, where ϵ is the dielectric constant, and m the electron effective mass. In units of the bare electron mass m_e one has $m = m^*m_e$. In this system of units, the length unit is the effective Bohr radius $a_0^* = a_0\epsilon/m^*$, and the energy unit is the effective Hartree $H^* = Hm^*/\epsilon^2$. In the numerical applications we have always considered GaAs, for which we have taken $\epsilon = 12.4$, $m^* = 0.067$, and $g^* = -0.44$. This yields $a_0^* \sim 97.94$ Å and $H^* \sim 11.86$ meV ~ 95.6 cm⁻¹. The Bohr magneton is $\mu_B = \hbar e/2m_e c$, and the cyclotron frequency is $\omega_c = eB/mc$.

The radial KS equations read

$$\begin{aligned} & \left[-\frac{1}{2} \left(\frac{d^2}{dr^2} + \frac{1}{r} \frac{d}{dr} - \frac{l^2}{r^2} \right) - \frac{\omega_c}{2} l + \frac{1}{8} \omega_c^2 r^2 - V^+(r) \right. \\ & \left. + V^H + V^{xc} + (W^{xc} + \frac{1}{2} g^* \mu_B B) \eta_\sigma \right] u_{nl\sigma} = \epsilon_{nl\sigma} u_{nl\sigma} , \end{aligned} \quad (1)$$

where $\eta_\sigma = +1(-1)$ for $\sigma = \uparrow(\downarrow)$, $V^H = \int d\vec{r}' n(\vec{r}')/|\vec{r} - \vec{r}'|$ is the Hartree potential, and $V^{xc} = \partial \mathcal{E}_{xc}(n, m)/\partial n|_{gs}$ and $W^{xc} = \partial \mathcal{E}_{xc}(n, m)/\partial m|_{gs}$ are the variations of the exchange-correlation energy density $\mathcal{E}_{xc}(n, m)$ written in terms of the electron density $n(r)$ and of the local spin magnetization $m(r) \equiv n^\uparrow(r) - n^\downarrow(r)$ taken at the ground state. $\mathcal{E}_{xc}(n, m)$ has been built from the 2DEG calculations of Tanatar and Ceperley¹⁹ at zero and full spin polarization, using the Von Barth and Hedin²⁰ interpolation formula adapted to 2D. The jellium potential $V^+(r)$ is analytical¹⁸:

$$V^+(r) = 4n_s \times \begin{cases} R_\infty \mathbf{E}(r/R_\infty) - R \mathbf{E}(r/R) & r < R \\ R_\infty \mathbf{E}(r/R_\infty) - r \mathbf{E}(R/r) + r [1 - (R/r)^2] \mathbf{K}(R/r) & r > R \end{cases} , \quad (2)$$

where \mathbf{K} and \mathbf{E} are the complete elliptic integrals of first and second kind, respectively²¹, and R_∞ represents a large r value. In practice, it is the largest- r used in the gs calculation. The KS differential equations have been solved without expanding the sp wave functions in a necessarily truncated basis of Landau orbitals. Our iterative method works for weak and strong B fields as well, for which the effective potential is very different. It has the advantage of avoiding to study how the results depend on the size of the basis. As in Ref. 22, we have worked at a small but finite temperature (0.1 K).

Physically acceptable solutions have to be regular at $r = 0$, and have to be bound due to the ω_c^2 term in the KS equation. Far from R they behave as^{23,24}

$$u_{nl\sigma}(r) \sim \left(\frac{r}{\mathcal{L}}\right)^{|l|} e^{-(r/2\mathcal{L})^2} L_n^{|l|} \left(\frac{r^2}{2\mathcal{L}^2}\right) , \quad (3)$$

where $\mathcal{L} \equiv \sqrt{\hbar/m\omega_c}$ is the magnetic length and $L_n^{|l|}$ is a generalized Laguerre polynomial²⁵.

Once the KS ground state has been obtained, we determine the dipole longitudinal response employing linear-response theory²⁶. We sketch here how the method is applied.

For independent electrons in the KS mean field, the variation $\delta n_\sigma^{(0)}$ induced in the spin density n_σ ($\sigma \equiv \uparrow, \downarrow$) by an external field F , whose non-temporal dependence we denote as $F = \sum_\sigma f_\sigma(\vec{r}) |\sigma\rangle\langle\sigma|$, can be written as²⁷

$$\delta n_\sigma^{(0)}(\vec{r}, \omega) = \sum_{\sigma'} \int d\vec{r}' \chi_{\sigma\sigma'}^{(0)}(\vec{r}, \vec{r}'; \omega) f_{\sigma'}(\vec{r}') , \quad (4)$$

where $\chi_{\sigma\sigma'}^{(0)}$ is the KS spin density correlation function. In this limit, the frequency ω corresponds to the harmonic time-dependence of the external field F and of the induced $\delta n_\sigma^{(0)}$. Eq. (4) is a 2×2 matrix equation in the two-component Pauli space. In longitudinal response theory, F is diagonal in this space, and its diagonal components are written as a vector $F \equiv \begin{pmatrix} f_\uparrow \\ f_\downarrow \end{pmatrix}$. We consider external dipole ($L = 1$) fields of the kind

$$F_{\pm 1}^{(n)} = f(r) e^{\pm i\theta} \begin{pmatrix} 1 \\ 1 \end{pmatrix} \quad \text{and} \quad F_{\pm 1}^{(m)} = f(r) e^{\pm i\theta} \begin{pmatrix} 1 \\ -1 \end{pmatrix} \quad (5)$$

which cause, respectively, charge and spin density modes of dipole type. To distinguish the induced densities in each excitation channel, we label them with an additional superscript as $\delta n_\sigma^{(0,n)}$ or $\delta n_\sigma^{(0,m)}$.

The TDLSDFT induced densities are obtained solving the integral equations

$$\delta n_\sigma^{(A)}(\vec{r}, \omega) = \delta n_\sigma^{(0,A)}(\vec{r}, \omega) + \sum_{\sigma_1 \sigma_2} \int d\vec{r}_1 d\vec{r}_2 \chi_{\sigma\sigma_1}^{(0)}(\vec{r}, \vec{r}_1; \omega) K_{\sigma_1 \sigma_2}(\vec{r}_1, \vec{r}_2) \delta n_{\sigma_2}^{(A)}(\vec{r}_2, \omega) , \quad (6)$$

where either $A = n$ or $A = m$, and the kernel $K_{\sigma\sigma'}(\vec{r}, \vec{r}')$ is the electron-hole interaction.

Equations (6) have been solved as a generalized matrix equation in coordinate space. Considering angular decompositions of $\chi_{\sigma\sigma'}$ and $K_{\sigma\sigma'}$ of the kind $K_{\sigma\sigma'}(\vec{r}, \vec{r}') = \sum_l K_{\sigma\sigma'}^{(l)}(r, r') e^{il(\theta-\theta')}$, it is enough to solve them for $l = 1$ because only this term couples to the external dipole field.

When a magnetic field is perpendicularly applied to the antidot, the ± 1 modes are not degenerate and two excitation branches may appear, each having *in principle* a different circular polarization, i.e., carrying an orbital angular momentum $\Delta L_z = \pm 1$, where L_z is that of the gs. In contradistinction with the quantum dot (QD) case, we will see that this is not so for antidots, for which the more intense peaks in both branches have the same polarization.

The induced charge or magnetization densities corresponding to density and spin responses are given by $\delta n^{(A)} = \delta n_\uparrow^{(A)} + \delta n_\downarrow^{(A)}$ and $\delta m^{(A)} = \delta n_\uparrow^{(A)} - \delta n_\downarrow^{(A)}$. From them, the dynamical polarizabilities in the density and spin channels are respectively given by

$$\begin{aligned} \alpha_{nn}(\omega) &= \int dr r f(r) \delta n^{(n)}(r) \\ \alpha_{mm}(\omega) &= \int dr r f(r) \delta m^{(m)}(r) . \end{aligned} \quad (7)$$

In this expression $\delta n^{(n)}$ has to be understood as the charge density induced by a spin-independent operator, and $\delta m^{(m)}$ as the spin density magnetization induced by a spin-dependent operator. Within longitudinal response theory, cross-channel induced densities such as $\delta m^{(n)}$ or $\delta n^{(m)}$ may also appear²⁶. The above expressions hold for each ± 1 circular polarization of the F operators defined in Eq. (5). Taking into account both possibilities, we define $\alpha_{AA}^{(1)}(\omega) \equiv \alpha_{AA}(1, \omega) + \alpha_{AA}(-1, \omega)$, whose imaginary part is proportional to the strength function $S_{AA}^{(1)}(\omega) = \text{Im}[\alpha_{AA}^{(1)}(\omega)]/\pi$. The peaks appearing in the strength functions are dipole charge density (CDE) or spin density excitations (SDE) caused by the external field. Analogously, the peaks appearing in the strength function which results from using in Eq. (7) the KS induced densities $\delta n_{\sigma}^{(0,A)}$ instead of the correlated ones $\delta n_{\sigma}^{(A)}$, correspond to dipole single particle excitations (SPE).

We have used for the $f(r)$ function entering Eq. (5) two different choices. One is the standard dipole operator $f(r) = r$, and the other one is $f(r) = 1/r$. As indicated in Ref. 18, the latter choice is inspired in the small-argument expansion of the irregular Bessel function $Y_1(qr)$. The relevance of this operator in the present context is that it mostly causes edge excitations. This will be further discussed in the next Section. The situation is analogous to that faced in the description of surface modes of 3D cavities in metals, see Ref. 28 for a thorough discussion.

III. RESULTS AND DISCUSSION

As a case of study we have considered an antidot of $n_s = 0.25 (a_0^*)^{-2}$ and $R = 7.5 a_0^*$. It roughly corresponds to one of the systems studied by Zhao et al² having $n_s = 2.6 \times 10^{11} \text{ cm}^{-2}$ and the same area. We recall that the antidot arrays studied in this reference have a very short period, whereas we have taken for R_{∞} defined in Eq. (2) a mean value of $30 a_0^*$, larger for large ν 's, and smaller for small ν 's. We have employed B values yielding integer filling factors $\nu = 2\pi n_s \mathcal{L}^2$ in the range $1 \leq \nu \leq 10$ which corresponds to $10.8 \geq B \geq 1.08$ T.

Figure 1 shows the particle $n(r)$ and spin magnetization densities $m(r)$ as a function of r for $\nu = 1$ to 6. Away from R , the electron density approaches n_s , and either $m(r)$ is zero if ν is even, or the local spin polarization $\xi(r) \equiv m(r)/n(r)$ equals $1/\nu$. The number of sp orbitals needed to numerically achieve this limit increases with ν , making it rather involved to obtain high- ν ground states. For instance, some 2500 occupied sp levels have been used to model the $\nu = 10$ gs.

Figure 2 shows the sp energies $\epsilon_{nl\sigma}$ as a function of l for the same configurations as in Fig. 1. In the bulk, $\epsilon_{nl\sigma}$ are arranged into Landau bands characterized by the index $M \equiv n + (|l| - l)/2$ and the value of σ . The filling factor represents the number of occupied Landau bands, each of them labeled as $(M, \uparrow \text{ or } \downarrow)$. It is worth noticing that since we have taken B in the positive z direction and the sp orbital angular momentum is written as $-l$, most occupied sp levels have $l \geq 0$, and that for a given M the (M, \uparrow) band lies below the (M, \downarrow) one.

These bands are almost degenerate when ν is even because of the smallness of the Zeeman energy and because $m(r) \simeq 0$ in the gs. When ν is odd, the spin dependence of the exchange-correlation energy \mathcal{E}_{xc} is responsible of the large gap between the $(M, \uparrow\downarrow)$ bands²⁹. Defining

the M -th Landau level as the set of (M, \uparrow) and (M, \downarrow) bands with $M = 0, 1, 2, \dots$, we see from Fig. 2 that even ν values correspond to completely filled Landau levels configurations, and odd ν values to configurations in which one Landau level is half-filled. If M is not too small, the M -th level is made of sp states having $n = M$. As in QD's, this rule is violated by a few sp states per Landau level at most, see for instance Fig. 1 of Ref. 29, and the $\nu = 6$ panel of Fig. 2.

The dipole FIR response has been obtained as outlined in Sect. II. Besides evaluating the occupied Landau levels, two more empty levels have been calculated, which allows an accurate description of modes up to $2\omega_c$. Figure 3 shows the charge, spin, and single electron strength functions corresponding to the dipole operator. All peaks displayed in this figure are of cyclotron-like type, i.e., they are excited by the $e^{+i\theta}$ component of the F operators in Eq. 5. This makes possible the transferring of strength among them, an effect that has been experimentally observed^{1,2}. We remark in passing that the fact that all these peaks originate from the same excitation operator makes the sum rule approach^{18,30} unsuitable to describe their excitation energies.

Our sign convention implies that at $B \neq 0$ the gs has a *negative* total orbital angular momentum L_z . Thus, these excitations *decrease* in one unit the absolute value of L_z ; whenever needed, we shall label cyclotron-like modes with a $(-)$ sign. Bulk magnetoplasmons in QD's also bear this character, whereas edge magnetoplasmons do not (see for instance Refs. 26,31). Indeed, edge magnetoplasmons in QD's are excited by the $e^{-i\theta}$ component of the dipole field and correspond to excitations which *increase* in one unit the absolute value of L_z . Whenever needed, we shall label the anticyclotron-like modes with a $(+)$ sign. The cyclotron-like character of edge magnetoplasmons in antidots has its microscopic origin in the upwards bending of the Landau levels for *small* l values, whereas the anticyclotron-like character of the edge magnetoplasmons in dots comes from the upwards bending of the Landau levels for *large* l values.

As in quantum dots, SDE's are weakly redshifted with respect to SPE's because of the attractive character of the rather small exchange-correlation vertex corrections, whereas CDE's are strongly blueshifted because of the repulsive character of the intense direct Coulomb interaction. In contradistinction with the QD case²⁶, no clear signature of a collective longitudinal spin edge magnetoplasmon appears at small B values: the edge spin mode is rather fragmented and weak. We recall that at full magnetization *longitudinal* spin and density responses coincide²⁶ and only spin modes of transverse type, not studied here, can be excited²⁹.

Another interesting feature of longitudinal response theory is that spin and charge density modes are generally coupled if the gs has a large spin magnetization, as it happens for instance at $\nu = 3$. This means that spin dependent probes may excite charge density modes. Conversely, spin independent probes may excite spin density modes. This coupling has been experimentally detected in QD's using Raman spectroscopy³², and has been theoretically addressed²⁶ within TDLSDF. For an antidot the effect is more marked, since ξ reaches $1/\nu$ instead of a smaller effective value as it happens in QD. This can be seen in Fig. 4.

It is worthwhile to compare antidot with dot results. For this sake, we show in Fig. 5 the dipole charge density response of a QD made of $N = 210$ electrons confined by the potential created by a jellium disk of radius $R \sim 16.7 a_0^*$. Outside the edge region, this system has a surface density of $\sim 0.24(a_0^*)^{-2}$, similar to our case-of study antidot, and it

has been thoroughly studied in Ref. 22. For this dot the $1 \leq \nu \leq 10$ range corresponds to $10.3 \geq B \geq 1.03$ T.

The energies of the more intense CDE's of the antidot and of the $N = 210$ QD have been drawn as a function of B in Figs. 6 and 7, respectively (a more complete version of Fig. 7 can be found in Ref. 26). Also drawn are the cyclotron frequency ω_c , and $2\omega_c$ and $3\omega_c$ as well. These figures show that the interaction of the bulk magnetoplasmon with the harmonics of the cyclotron resonance $n\omega_c$, resembling the Bernstein modes³³, which causes the splitting of the magnetoplasmon near $2\omega_c$ and $3\omega_c$, is well reproduced by the calculations. Alongside the groups of peaks corresponding to CDE's we have indicated the change in radial quantum number n of the sp wave functions involved in the transition. This change Δn is unambiguously identified in TDLSDFT calculations introducing energy cutoffs in the electron-hole energy denominators $\Delta\epsilon$ entering the definition of the free correlation function²⁶ $\chi_{\sigma\sigma}^{(0)}$: limiting the electron-hole pairs to those having $\Delta\epsilon < \omega_c$, only $\Delta n = 0$ peaks appear in the response, whereas limiting them to those with $\Delta\epsilon < 2\omega_c$, no $\Delta n = 2$ peaks appear. These cyclotron-like $\Delta n = 2$ peaks have been experimentally detected⁹.

The correlations introduced by TDLSDFT have a dramatic effect on the FIR response of the system which might not always be properly recognized. Not only they appreciably shift the CDE energies with respect to the SPE's but also affect their intensity, causing that peaks having a sizeable strength in the SPE response are nearly washed out, whereas others hardly perceived in the SPE response acquire a large strength. To illustrate it we show in Fig. 8 the single particle and charge density strength functions for $\nu = 7$ in a logarithmic scale. It can be noticed that in the SPE strength the $2\omega_c$ peak, which has an intensity six orders of magnitude smaller than the ω_c peak and cannot be seen at the scale of Fig. 3, emerges as a very collective peak in the CDE strength, of intensity similar to that of the bulk $\Delta n = 1$ peak. Similarly, the weak edge SPE's loose their dimy intensity, transferring it to the very collective $\Delta n = 0$ edge CDE. Of course, in actual TDLSDFT calculations all these modes are reciprocally influenced, but the gross effect is as described.

TDLSDFT does reproduce the oscillation of the edge magnetoplasmon energy as a function of filling factor¹². Figure 9 shows the edge magnetoplasmon energy as a function of ν for the antidot and the $N = 210$ dot. The oscillations and the out-of-phase effect¹² are tiny effects better seen plotting the second differences of the edge magnetoplasmon energy:

$$\Delta_2\omega(\nu) = \omega(\nu + 1) - 2\omega(\nu) + \omega(\nu - 1) . \quad (8)$$

The energy oscillations are clearly seen in the Fig. 9 insert, as well as the experimental finding that maxima in the edge magnetoplasmon energies correspond to half-filled Landau levels in antidots, and to filled Landau levels in dots.

From Figs. 3 and 6 we conclude that for an isolate antidot, TDLSDFT is unable to produce the anticrossing of the edge and the cyclotron modes at small B values which is observed in short-period antidot arrays. Yet, the behavior of the antidot and dot $\Delta n = 0$ edge branch near the crossing is quite distinct, manifesting a different curvature. The low- B behavior of the edge brach experimentally found in short-period antidot arrays is likely influenced by neighboring antidots. Notice that $\mathcal{L} \sim 1.9 a_0^*$ at $\nu = 6$, which is roughly half the effective surface width of the antidot lattice period of Ref. 2.

Figures 3 and 6 also show that the TDLSDFT antidot response is very fragmented at low B . This renders tricky to distinguish bulk from edge charge modes. Notice that at

$\nu = 10$ the high energy peak in Fig. 3 is a $\Delta n = 2$ mode, whereas the low energy peak is a mixture of $\Delta n = 0$ and $\Delta n = 1$ peaks. The situation worsens increasing ν , which is beyond our capabilities. For instance, to have results at $B \sim 0.5$ T one would need to carry out calculations for $M \sim 20$.

A possible way to partially disentangle these modes is to study the charge density response to the $f(r) = 1/r$ operator. Its r dependence makes this very ineffective in exciting cyclotron-like modes while it is well suited to describe edge oscillations. This can be seen in Fig. 10, where we have plotted the CDE's caused by r and $1/r$ for $\nu = 10$ to 7. In the bottom panel, the intensity of the $1/r$ peaks has been multiplied by a factor of 50,000 to allow for a sensible comparison with the r peaks. It can then be seen in that panel that both operators excite the same $\Delta L_z = +1$ peaks, but with much different intensity, and that indeed, the low energy peak clearly visible in the response is an edge peak.

Finally, we have plotted in the top panel of that figure the CDE caused by the $e^{-i\theta}$ component of the F operators in Eq. 5. These are anticyclotron-like excitations of very weak intensity: to have them at the same scale as in the bottom panel, one should divide the scale of the r modes by a factor of 40, and the scale of the $1/r$ modes by a factor of 4, i.e., the $1/r$ operator excites the cyclotron-like and anticyclotron-like main peaks with roughly equal intensity. In agreement with the experiment (see especially Fig. 1 of Ref. 9), it can be seen on the one hand that their intensity quickly decrease as B increases, and on the other hand that their energies are very similar to these of the cyclotron-like modes. This makes these modes experimentally accessible only using circular polarized radiation.

IV. ACKNOWLEDGMENTS

It is a pleasure to thank Vidar Gudmundsson for useful discussions. This work has been performed under grants PB98-1247 and PB98-0124 from DGESIC, and SGR98-00011 from Generalitat of Catalunya. A.E. acknowledges support from the Dirección General de Enseñanza Superior (Spain).

REFERENCES

- ¹ K. Kern, D. Heitmann, P. Grambow, Y. H. Zhang, and K. Ploog, Phys. Rev. Lett. **66**, 1618 (1991).
- ² Y. Zhao, D. C. Tsui, M. Santos, M. Shayegan, R. A. Ghanbari, D. A. Antoniadis, and H. I. Smith, Appl. Phys. Lett **60**, 1510 (1992).
- ³ A. Lorke, I. Jejina, and J. P. Kotthaus, Phys. Rev. B **46**, 12845 (1992).
- ⁴ C. Dahl, J. P. Kotthaus, H. Nickel, and W. Schlapp, Phys. Rev. B **48**, 15480 (1993).
- ⁵ A. Emperador, M. Barranco, E. Lipparini, M. Pi, and Ll. Serra, Phys. Rev. B **59**, 15311 (1999).
- ⁶ K. Bollweg, T. Kurth, D. Heitmann, E. Vasiliadou, and K. Ebert, Phys. Rev. B **52**, 8379 (1995).
- ⁷ Ch. Sikorski and U. Merkt, Phys. Rev. Lett. **62**, 2164, (1989).
- ⁸ T. Demel, D. Heitmann, P. Grambow, and K. Ploog, Phys. Rev. Lett. **64**, 788 (1990).
- ⁹ M. Hochgräfe, R. Krahne, Ch. Heyn, and D. Heitmann, Phys. Rev. B **60**, 10680 (1999).
- ¹⁰ G. Y. Wu and Y. Zhao, Phys. Rev. Lett. **71**, 2114 (1993).
- ¹¹ S. A. Mikhailov and V. A. Volkov, Phys. Rev. B **52**, 17260 (1995).
- ¹² K. Bollweg, T. Kurth, D. Heitmann, V. Gudmundsson, E. Vasiliadou, P. Grambow, and K. Ebert, Phys. Rev. Lett. **76**, 2774 (1996).
- ¹³ V. Fessatidis, H. L. Cui, and O. Kün, Phys. Rev. B **47**, 6598 (1993).
- ¹⁴ S. A. Mikhailov, Phys. Rev. B **54**, R14293 (1996).
- ¹⁵ D. Huang and G. Gumbs, Phys. Rev. B **47**, 9597 (1993).
- ¹⁶ V. Gudmundsson and R. R. Gerhardts, Phys. Rev. B **54**, R5223 (1996).
- ¹⁷ V. Gudmundsson, Phys. Rev. B **57**, 3989 (1998).
- ¹⁸ A. Emperador, M. Pi, M. Barranco, E. Lipparini, and Ll. Serra, Phys. Rev. B **58**, 6732 (1998).
- ¹⁹ B. Tanatar and D. M. Ceperley, Phys. Rev. B **39**, 5005 (1989)
- ²⁰ U. von Barth and L. Hedin, J. Phys. C **5**, 1629 (1972).
- ²¹ I.S. Gradshteyn and I.M. Ryzhik, *Table of Integrals, Series and Products*, Academic Press, New York (1980).
- ²² M. Pi, M. Barranco, A. Emperador, E. Lipparini, and Ll. Serra, Phys. Rev. B **57**, 14783 (1998).
- ²³ V. Fock, Z. Phys. **47**, 446 (1928).
- ²⁴ C. G. Darwin, Proc. Cambridge Philos. Soc. **27**, 86 (1930).
- ²⁵ M. Abramowitz and I. A. Stegun, *Handbook of Mathematical Functions* (Dover Pu., New York, 1970).
- ²⁶ Ll. Serra, M. Barranco, A. Emperador, M. Pi, and E. Lipparini, Phys. Rev. B **59**, 15290 (1999).
- ²⁷ A.R. Williams and U. von Barth, *Theory of the Inhomogenous Electron Gas*, edited by S. Lundqvist and N. H. March (Plenum, New York, 1983) p. 231.
- ²⁸ Ll. Serra, F. Garcias, J. Navarro, N. Barberan, M. Barranco, and M. Pi, Phys. Rev. B **46**, 9369 (1992).
- ²⁹ E. Lipparini, M. Barranco, A. Emperador, M. Pi, and Ll. Serra, Phys. Rev. B **60**, 8734 (1999).
- ³⁰ E. Lipparini, N. Barberan, M. Barranco, M. Pi, and Ll. Serra, Phys. Rev. B **56**, 12375 (1997).

³¹ V. Gudmundsson and R. R. Gerhardts, Phys. Rev. B **43**, 12098 (1991).

³² C. Schüller, K. Keller, G. Biese, E. Ulrichs, L. Rolf, C. Steinebach, D. Heitmann, and K. Eberl, Phys. Rev. Lett. **80**, 2673 (1998).

³³ V. Gudmundsson, A. Brataas, P. Grambow, B. Meurer, T. Kurth, and D. Heitmann, Phys. Rev. B **51**, 17744 (1995).

FIGURES

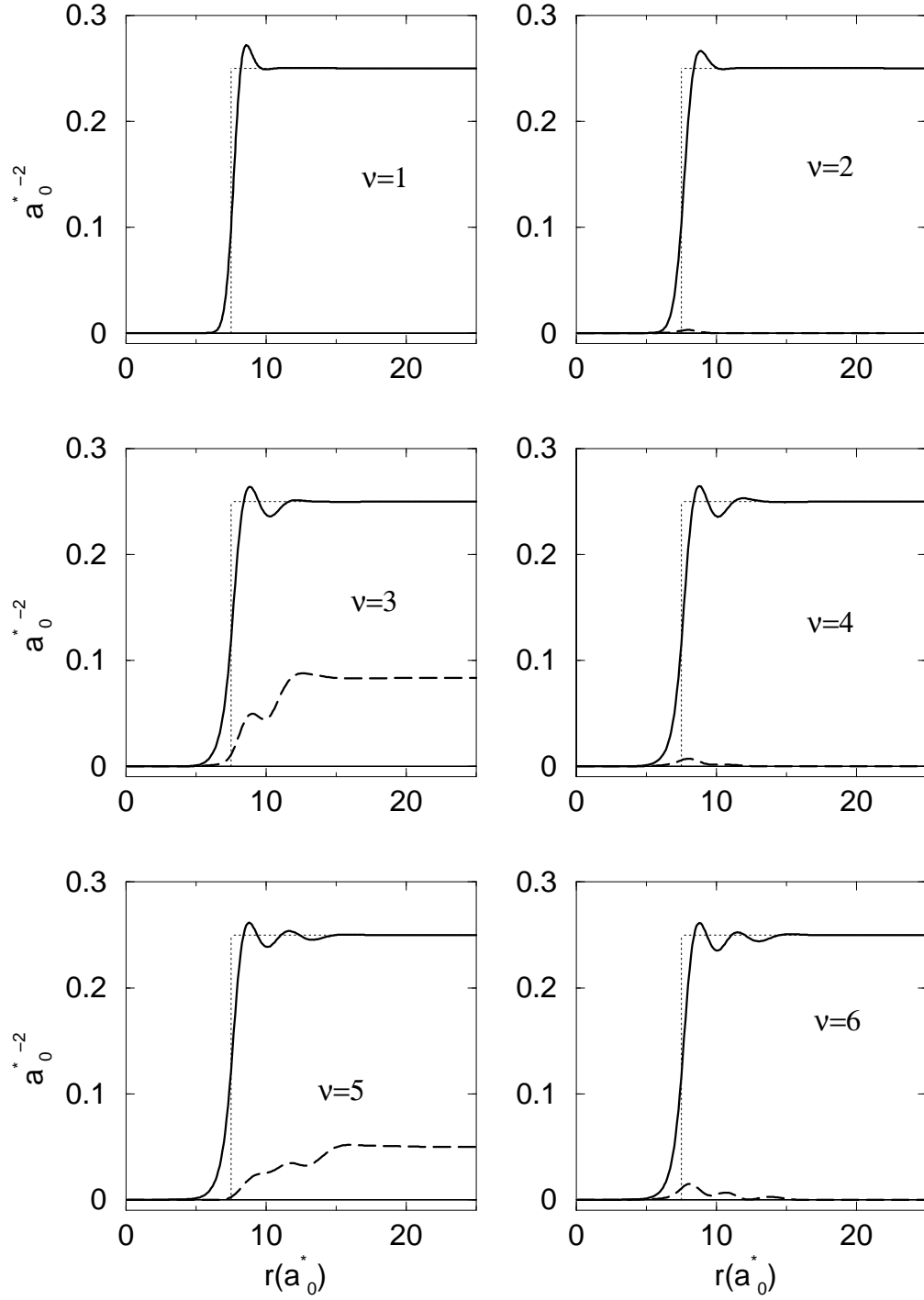


FIG. 1. Electron (solid lines) and spin magnetization (dashed lines) densities as a function of r for an antidot of $R = 7.5 a_0^*$ and $n_s = 0.25 (a_0^*)^{-2}$ and several filling factors. Also shown is the jellium density (dotted lines).

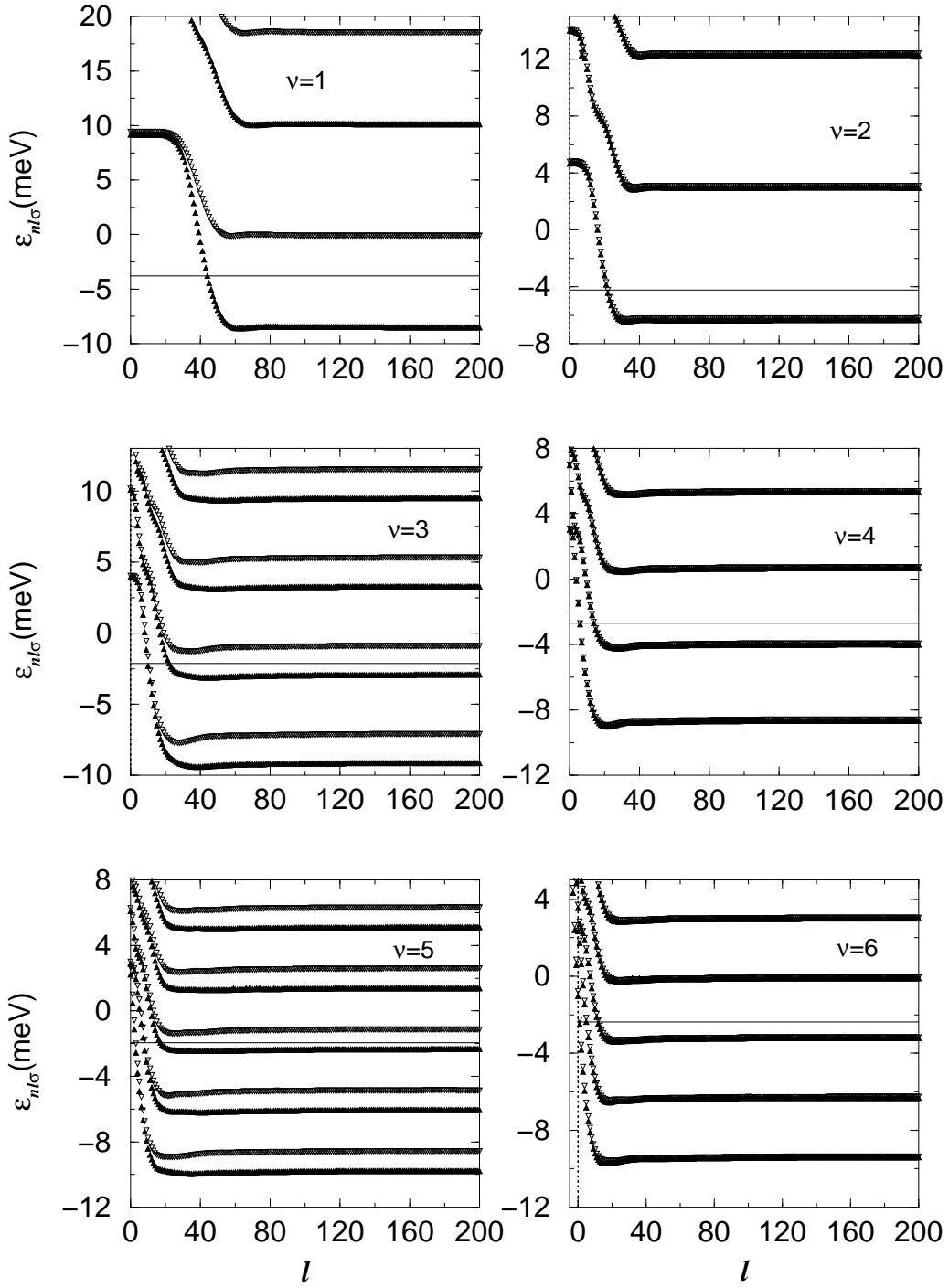


FIG. 2. Single particle energies $\epsilon_{nl\sigma}$ as a function of l for the configurations of Fig. 1. The horizontal line represents the electron chemical potential. Full upright triangles represent (M, \uparrow) bands, and empty downright triangles represent (M, \downarrow) bands.

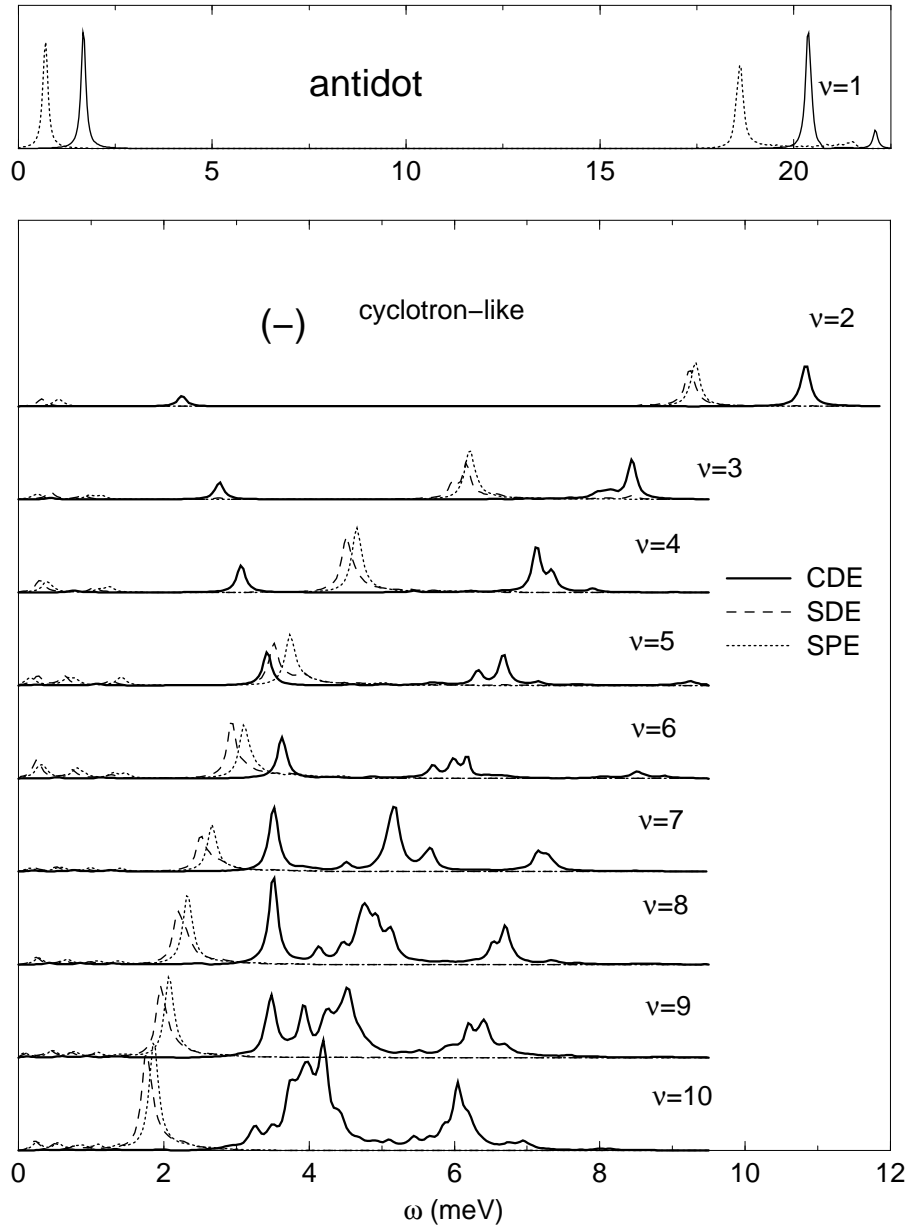


FIG. 3. Charge, spin, and single particle antidot dipole strength functions in arbitrary units. All displayed modes are cyclotron-like polarized $(-)$. Notice the different energy scale of the $\nu = 1$ responses.

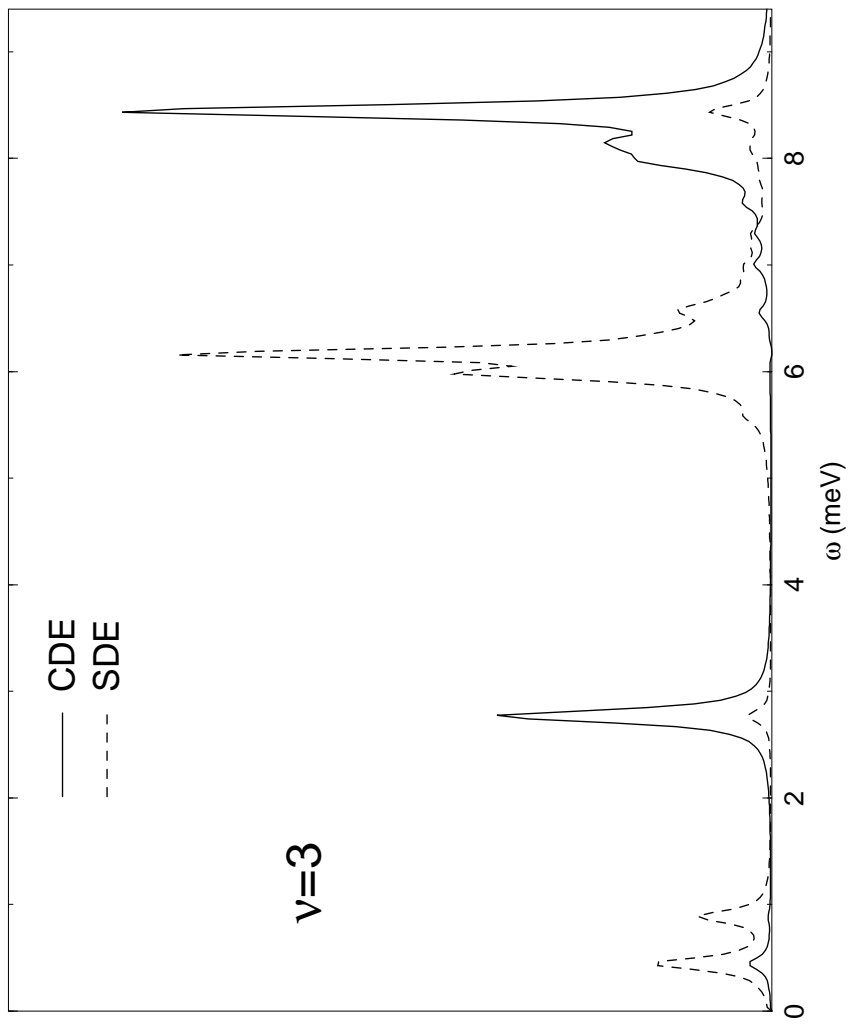


FIG. 4. Charge and spin antidot dipole strength functions at $\nu = 3$ in arbitrary units illustrating the coupling between the strengths at high spin magnetizations.

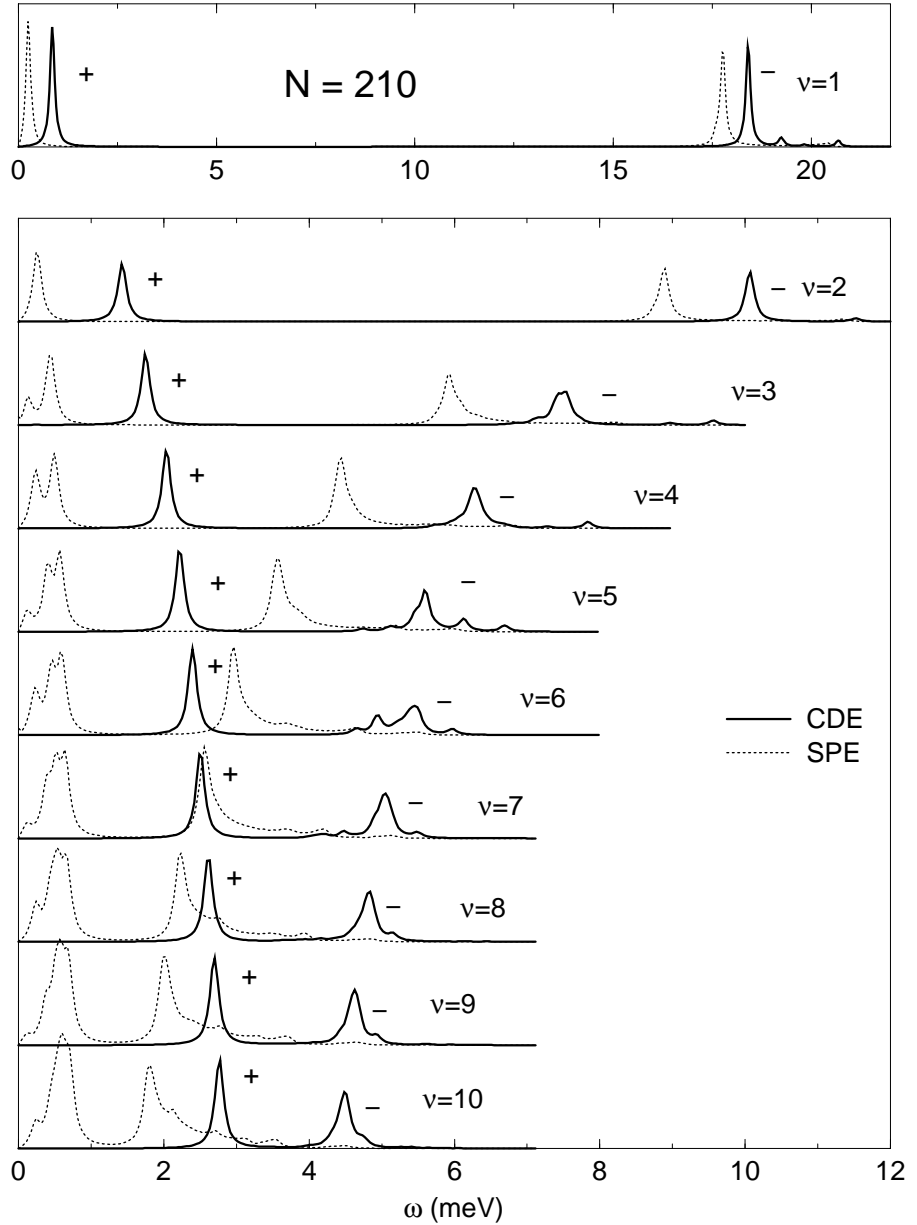


FIG. 5. Charge and single particle dipole strength functions in arbitrary units corresponding to the $N = 210$ dot described in the text. Cyclotron-like polarized (–) bulk modes and anticyclotron polarized (+) edge modes appear in the responses. Notice the different energy scale of the $\nu = 1$ responses.

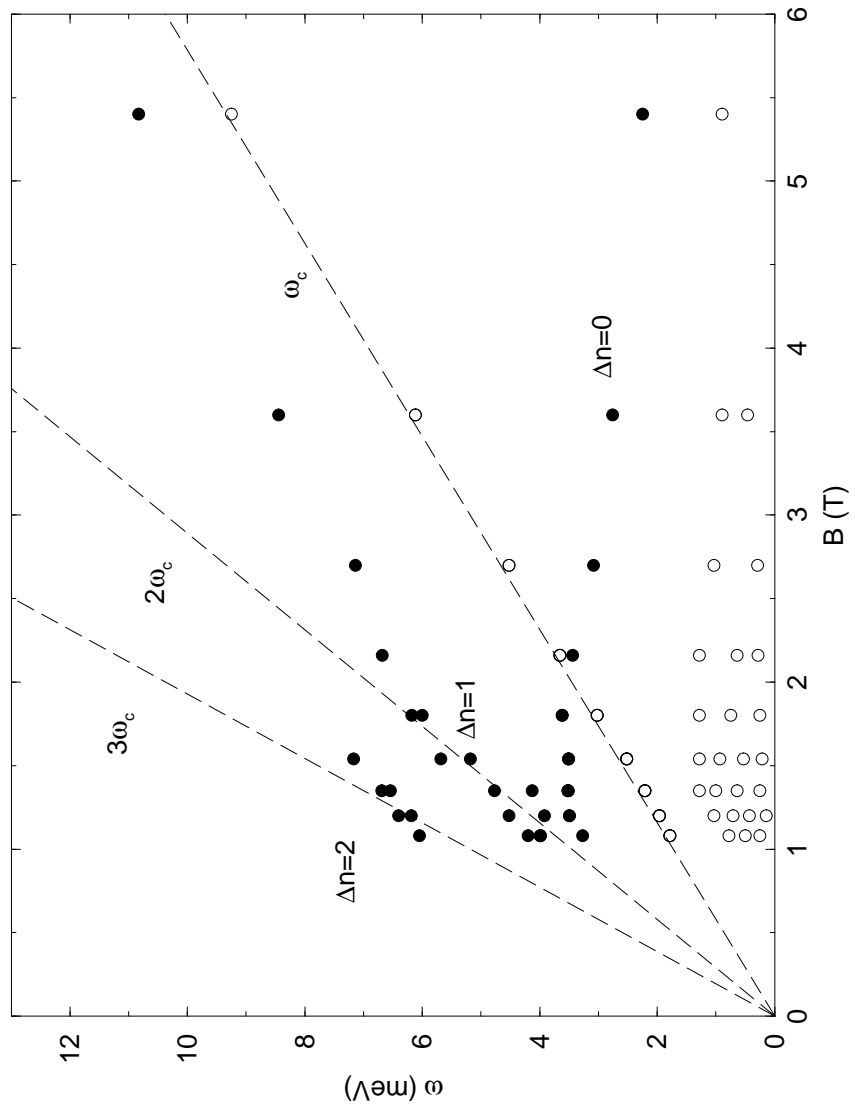


FIG. 6. Energies of the more intense antidot CDE's (solid circles) and SDE's (open circles) as a function of B . From left to right, the calculated points correspond to $\nu = 10$ to 2.

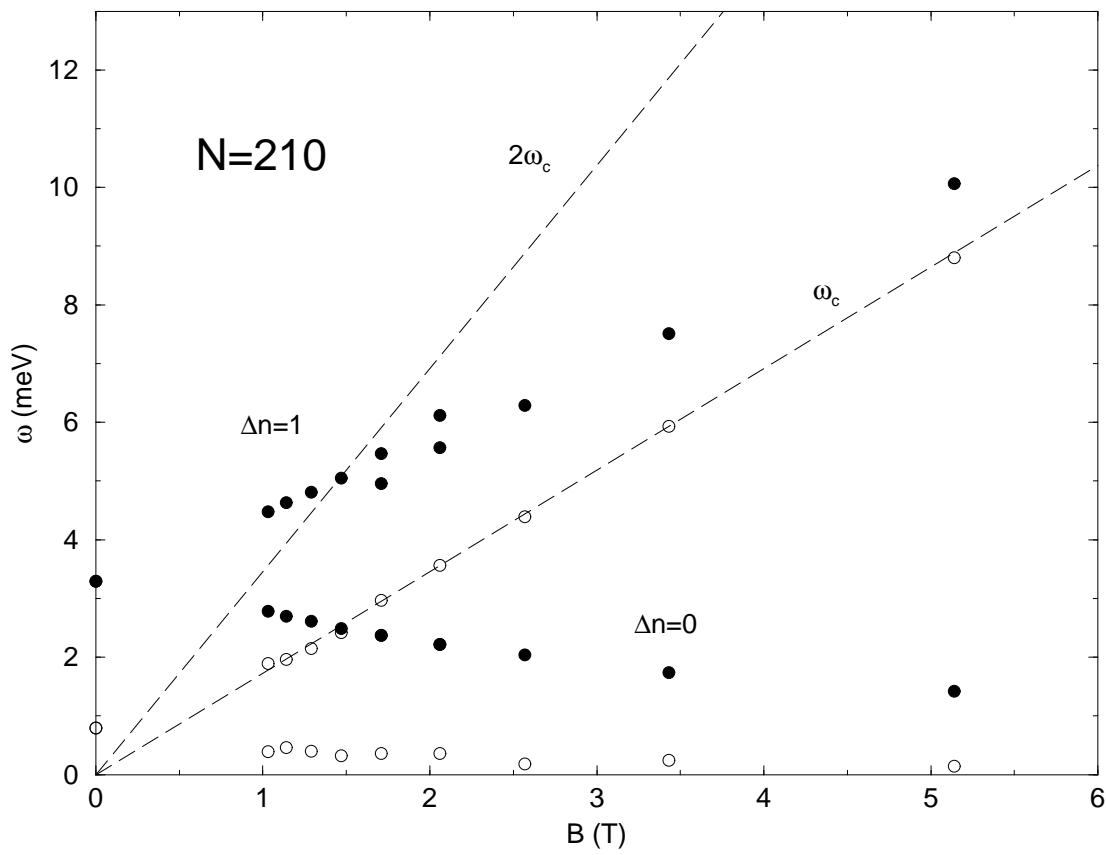


FIG. 7. Same as Fig. 6 for the $N = 210$ dot. Also drawn are the $B = 0$ values

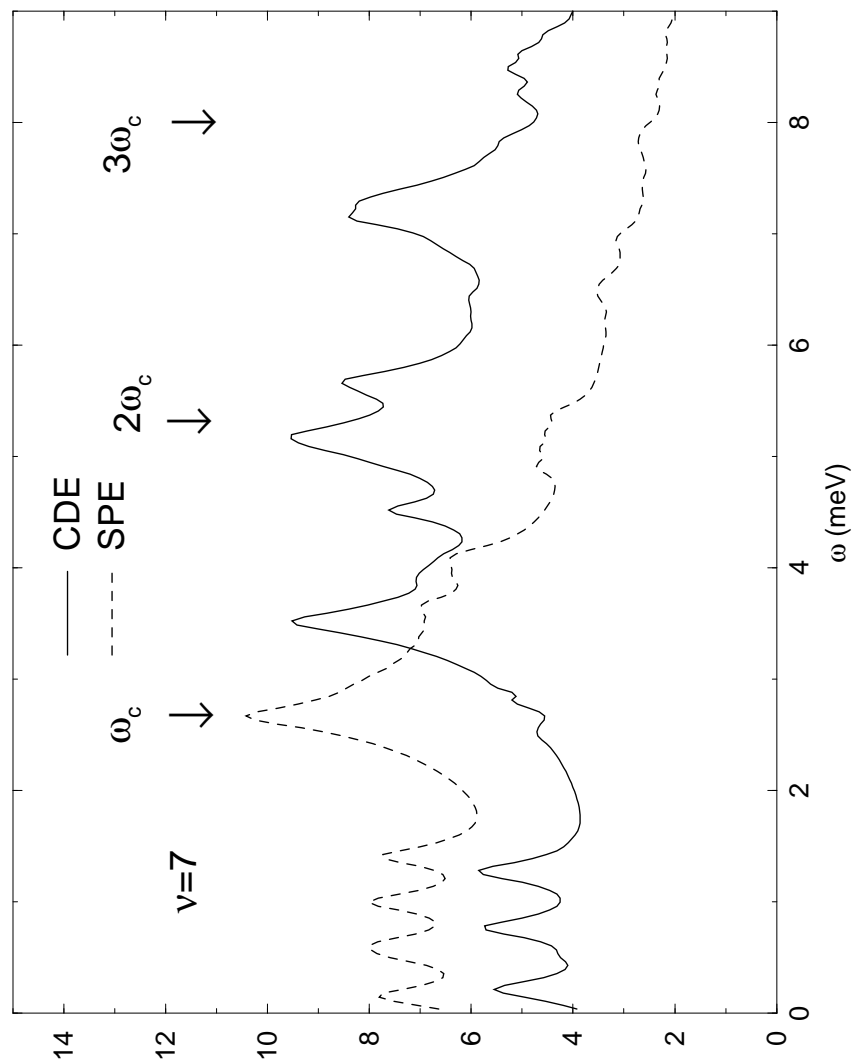


FIG. 8. Antidot CDE (solid line) and SPE (dashed line) strength functions at $\nu = 7$ in a logarithmic scale.

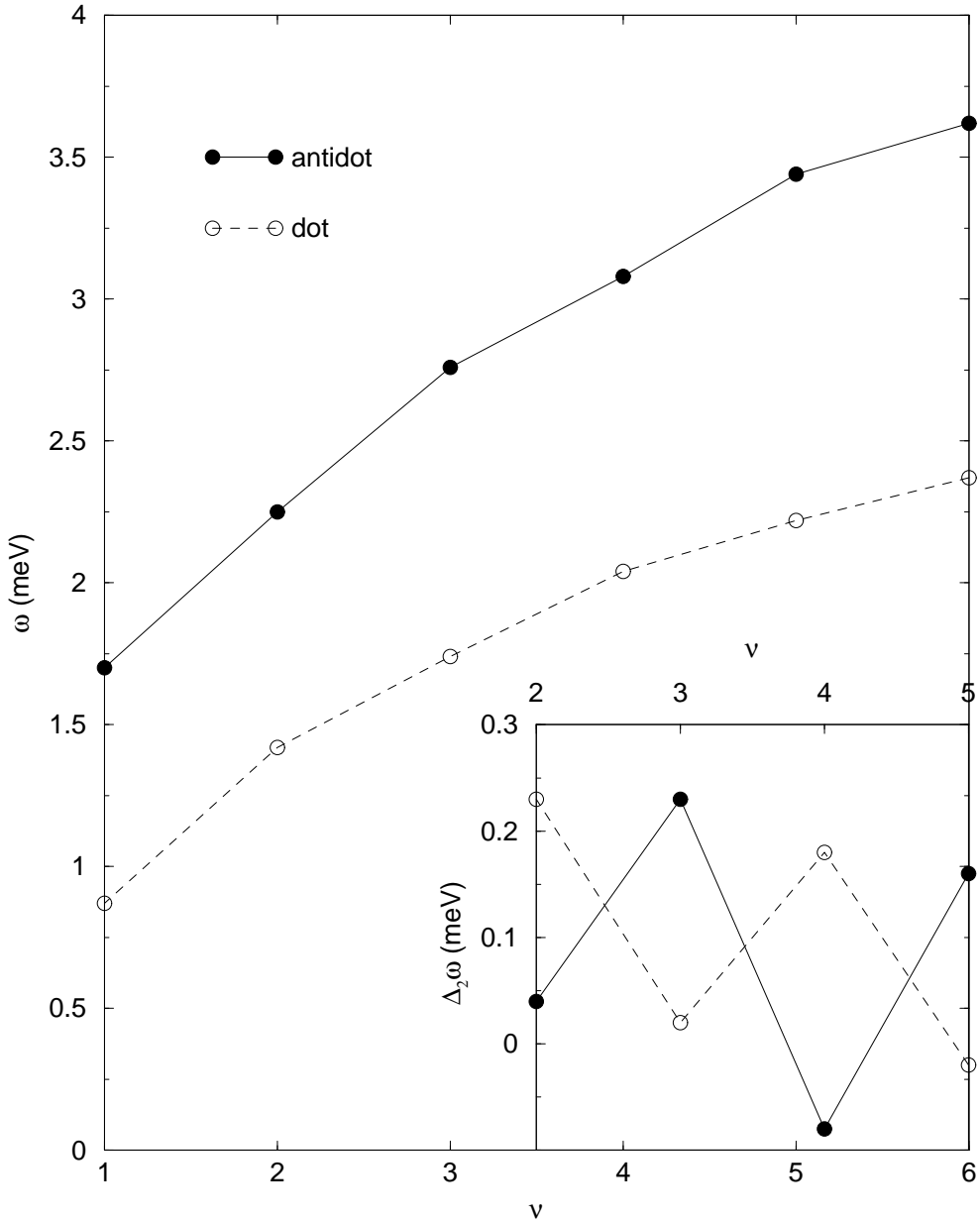


FIG. 9. Edge magnetoplasmon energies of the antidot (solid circles) and of the $N = 210$ dot (open circles) as a function of filling factor. The insert displays the second differences $\Delta_2 \omega$. The lines have been drawn to guide the eye.

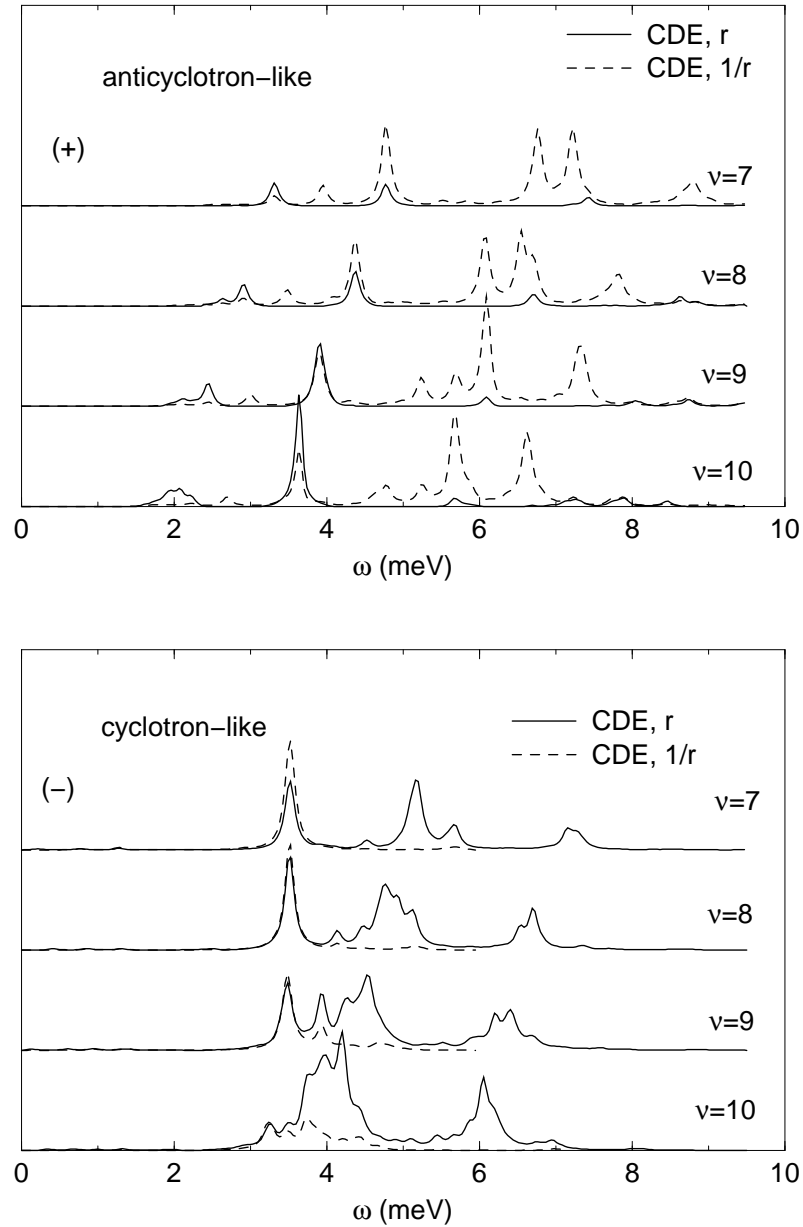


FIG. 10. Antidot charge density strength functions in arbitrary units for $\nu = 10$ to 7 caused by r (solid lines) and $1/r$ (dashed lines) fields. Top panel, anticyclotron-like polarized (+) modes. Bottom panel, cyclotron-like polarized (-) modes.